Chinese Physics Letters **39**, 123201 (2022) **Express Letter**

Real-Time Observation of Electron-Hole Coherence Induced by Strong-Field Ionization

Jing Zhao(赵晶)[1], Jinlei Liu(刘金磊)[1], Xiaowei Wang(王小伟)[1], Jianmin Yuan(袁建民)[1,2], and Zengxiu Zhao(赵增秀)[1*]

[1]*Department of Physics, National University of Defense Technology, Changsha 410073, China*
[2]*Graduate School of China Academic of Engineering Physics, Beijing 100193, China*

(Received 20 October 2022; accepted manuscript online 23 November 2022)

We introduce and demonstrate a new approach to measure the electron-hole dynamics and coherence induced by strong-field ionization using hole-assisted high-harmonic spectroscopy. The coherent driving of the infrared and XUV pulses correlates the dynamics of the core-hole and the valence-hole by coupling multiple continua, which leads to the otherwise forbidden absorption and emission of high harmonics. An analytical model is developed based on the strong-field approximation by taking into account the essential multielectron configurations. The emission spectra from the core-valence transition and the core-hole recombination are found to modulate strongly as functions of the time delay between the two pulses, suggesting that the coherent electron wave packets in multiple continua can be utilized to temporally resolve the core-valence transition in attoseconds.

DOI: 10.1088/0256-307X/39/12/123201

Recent advances in attosecond spectroscopy have enabled researchers to resolve electron-hole dynamics in real time.[1–8] The correlated electron-hole dynamics and the resulted coherence are directly related to how fast the ionization is completed.[1,2,9,10] Combining the ever-shorter attosecond pulses with intense infrared lasers, it is possible to probe and control both core and valence electrons coherently on the equal footing. However, it is still of challenge to answer these key questions in attosecond physics or even attosecond chemistry,[11–15] such as how the coherence evolves and transfers among electron-hole pairs or multiple channels.

Coherent x-ray pulses with duration of femtosecond or attoseconds have been generated from free-electron lasers[16,17] or high-harmonic generation (HHG).[18–20] They are capable of creating inner holes followed with exotic correlated electron dynamics such as cascading Auger processes[3–5,21] and ionization induced absorption saturation.[22,23] On the other hand, intense infrared (IR) lasers ignite ionization from the valence shell. The released electron and the created hole are still driven by the external fields. When the field reverse its direction, the electron recombines into the original hole leading to HHG. However, due to the multielectron nature, many-body effects, e.g., dynamical polarization,[24,25] will modify the dynamics of both electrons and holes. Particularly, previous work has demonstrated that multielectron information is encoded in HHG when inner shell electrons are excited by the IR lasers and participate in the ultrafast dynamics,[26–33] while the effect on HHG from coherent driving of core-valence transition by attosecond pulses remains unexplored.

In this work, we consider a unique scenario involving atoms with closed shells subjected to an intense IR laser pulse and a time-delayed attosecond pulse (AP) which has a central frequency in resonance with the transition between the inner and valence shells. In the absence of the IR pulse, the direct transition from the inner shell to the valence shell is forbidden due to the Pauli exclusion principle. However, once the IR field induces ionization from the valence shell, the transition is triggered to leave a hole in the inner shell affecting the subsequent rearrangement dynamics. As shown in Fig. 1, strong field ionization from the filled valence shell by IR field creates the associated continuum. Concurrently, it opens the subshell allowing the followed resonant transition pumped by the AP, which creates a hole in the core and transfers the continuum into its own. The attosecond light absorption and the resulted emission are thus gated by the ionization, in close analogy to the ionization induced absorption saturation where the transition energy is shifted by ionization.[23] Meanwhile, the opened AP absorption creates coherence between the valence-hole and core-hole states. The transfer of coherence from ionization into both holes leads to multiple paths of HHG: harmonics can be radiated through recombination into the valence shell (path v) and the core hole (path h) respectively, or it can be generated upon the resonant core-valence transition accompanied by the transfer of the continua (path x). The coherent electron wave packet in multiple continua thus provides the opportunity to temporally resolve the multi-electron-hole dynamics in attoseconds.

To describe the multi-electron dynamics, we develop an analytical model by including the essential multielectron configurations involved, i.e., the neutral ground state $\Psi_{\rm g}$, the nonstationary state Ψ_1^* which constitutes of the ionic ground state Φ_1' with the nth electron in the continuum $\psi_v(\boldsymbol{r}_n, t)$, and the nonstationary state Ψ_2^* with the ionic

*Corresponding author. Email: zhaozengxiu@nudt.edu.cn
© 2022 Chinese Physical Society and IOP Publishing Ltd

core in excited state Φ_2' and the released electron in the continuum $\psi_h(\boldsymbol{r}_n, t)$. Taking the Ne atom as an example, we have $\Phi_1' = \Phi_{1s^2 2s^2 2p^5}$ and $\Phi_2' = \Phi_{1s^2 2s^1 2p^6}$, which can be formed by ionization from the valence shell or inner shell, respectively. The total time-dependent wave function of the N-electron atom can thus be approximated as

$$\begin{aligned}\Psi(t) = a_{\rm g}(t)\Psi_{\rm g} e^{-iE_{\rm g}t} + \hat{\mathcal{A}}[\Phi_1'\psi_v(t)]e^{-iE_1' t} \\ + \hat{\mathcal{A}}[\Phi_2'\psi_h(t)]e^{-iE_2' t},\end{aligned} \tag{1}$$

where $\hat{\mathcal{A}} = (1 - \sum_{i=1}^{n-1} \hat{P}_{in})/\sqrt{n}$ is the antisymmetrizing operator on the electron coordinates with $\hat{P}_{in}$ interchanging the cationic electron i and the nth electron. $E_{\rm g}$, E_1', and E_2' are the binding energies of the neutral ground state, the ionic ground state, and excited state, respectively, which are the Hartree–Fock single-slater determinants. The continuum electron is described by a superposition of plane waves in spirit of the strong-field approximation,[34] assuming that the continuum electron feels mainly the force of the laser field, while the effect of the Coulomb potential is ignored when treating the strong interaction with the laser field. The probabilities of finding the ion in the ground or excited states are given by the normalization of the continuum electrons, denoted by $||\psi_v||^2$ and $||\psi_h||^2$ respectively. The probability amplitude of the atom remaining in the neutral ground state is denoted by $a_{\rm g}$, and $|a_{\rm g}|^2 + ||\psi_v||^2 + ||\psi_h||^2 = 1$.

The time evolution of the N-electron atom under the influence of a linearly polarized electromagnetic field $\boldsymbol{E}(t)$ is governed by the time-dependent Schrödinger equation

$$i\frac{\partial}{\partial t}\Psi(t) = \Big[H_0 + \sum_{i=1}^{n} \boldsymbol{r}_i \cdot \boldsymbol{E}(t)\Big]\Psi(t), \tag{2}$$

with H_0 being the field-free Hamiltonian of the atom. Dipole approximation is applied for the laser-atom interaction. Considering that the binding electrons are localized and the free electron accelerated by the strong field has large momentum, the overlap between them can be assumed vanishing, therefore the exchange effect arising from the exchange of the free electron with the binding electrons is neglected. Using the orthogonality among the three configurations and neglecting the temporal variation of ground-state population, we obtain the coupled-channel equations for the nth electron,

$$\begin{aligned}i\dot{\psi}_v = \tilde{H}_v\psi_v + a_{\rm g}(t)\langle\Phi_1'|\boldsymbol{r}\cdot\boldsymbol{E}(t)|\Psi_{\rm g}\rangle' e^{iI_1 t} \\ + \Big\langle\Phi_1'|\sum_{i=1}^{n-1}\boldsymbol{r}_i\cdot\boldsymbol{E}(t)|\Phi_2'\Big\rangle'\psi_h e^{-i\Delta I t},\end{aligned} \tag{3}$$

$$\begin{aligned}i\dot{\psi}_h = \tilde{H}_h\psi_h + a_{\rm g}(t)\Big\langle\Phi_2'|\boldsymbol{r}\cdot\boldsymbol{E}(t)|\Psi_{\rm g}\Big\rangle' e^{iI_2 t} \\ + \Big\langle\Phi_2'|\sum_{i=1}^{n-1}\boldsymbol{r}_i\cdot\boldsymbol{E}(t)|\Phi_1'\Big\rangle'\psi_v e^{i\Delta I t},\end{aligned} \tag{4}$$

where $\langle|\cdots|\rangle'$ denotes the integration over the $(n-1)$-electron coordinates, $I_{1,2} = E_{1,2}' - E_{\rm g}$ and $\Delta I = I_2 - I_1$. For simplicity, we have replaced $\boldsymbol{r}_n$ by $\boldsymbol{r}$. $\tilde{H}_{v,h}$ are the effective Hamiltonians for the excited electron in the laser field with the core left in the two ionic states, respectively,

$$\tilde{H}_v = H_v + \langle\Phi_1'|H_{\rm I}|\Phi_1'\rangle' + \boldsymbol{r}\cdot\boldsymbol{E}(t), \tag{5}$$

$$\tilde{H}_h = H_v + \langle\Phi_2'|H_{\rm I}|\Phi_2'\rangle' + \boldsymbol{r}\cdot\boldsymbol{E}(t), \tag{6}$$

where H_v is the field-free Hamiltonian of the nth electron, and $H_{\rm I}$ represents the interaction between the continuum electron and the two ionic cores. The second terms in Eqs. (3) and (4) describe the transition from the neutral ground state to the two ionic states by prompting the nth electron into their respective continuum, while the third terms represent the couplings between the two ionic channels induced by the external fields.

We consider the dynamics of the multielectron system driven by the combination of a strong infrared laser field $\boldsymbol{E}_{\rm L}(t)$ and an attosecond XUV pulse $\boldsymbol{E}_{\rm X}(t)$ with the total field given by $\boldsymbol{E}(t) = \boldsymbol{E}_{\rm L}(t) + \boldsymbol{E}_{\rm X}(t)$. The central frequency of the XUV pulse is chosen to be exactly matching the transition energy ΔI from the inner shell to the valence shell. Clearly, when the valence shell is fully occupied, the transition from the inner shell to the valence shell is prohibited. However, once the strong laser field induces ionization which removes the electron from the valence shell, the transition starts to occur with the rate proportional to $||\psi_v||^2$. Since the laser frequency is far less than the transition energy ΔI, its contribution to the core-valence transition is negligible unless multiphoton resonant excitation occurs, which is not the case considered here. Therefore, for ionization from the valence shell [Eq. (3)], we include only direct ionization from the neutral ground state by the intense laser field, while neglecting the population variation of the valence shell induced by the core excitation with the AP. For the core hole creation [Eq. (4)], the direct excitation from the neutral ground state is negligible and we consider only the coupling between the two ionic channels. Denoting the respective Green's functions $\tilde{H}_v$ and $\tilde{H}_h$ as $\tilde{G}_v$ and $\tilde{G}_h$, we obtain

$$\psi_v(t) = \int^t dt' \tilde{G}_v(t,t') a_{\rm g}(t') \boldsymbol{E}_{\rm L}(t') e^{iI_1 t'} \langle\Phi_1'|\boldsymbol{r}|\Psi_{\rm g}\rangle', \tag{7}$$

$$\psi_h(t) = \int^t dt' \tilde{G}_h(t,t') \boldsymbol{d}_{12}^* \boldsymbol{E}_{\rm X}(t') e^{i\Delta I t'} \psi_v(t'). \tag{8}$$

The core-valence transition dipole moment between the two ionic states Φ_1' and Φ_2' is given by $\boldsymbol{d}_{12} = (n-1)\langle\Phi_1'|\sum_{i=1}^{n-1}\boldsymbol{r}_i|\Phi_2'\rangle'$. In Green's function, we include the laser field which has dominant effect on the continuum electron, and neglect the contribution of the atomic potential within the strong-field approximation. Green's function can be written in term of Volkov states $\phi_{\boldsymbol{p}}^{\rm V}(t) = e^{-iS(\boldsymbol{p},t,t')} e^{i[\boldsymbol{p}+\boldsymbol{A}(t)]\cdot\boldsymbol{r}}$, describing a plane-wave state with time-dependent electron momentum $\boldsymbol{p} + \boldsymbol{A}(t)$, where the semiclassical action is $S(\boldsymbol{p},t,t') = \int_{t'}^{t} \frac{[\boldsymbol{p}+\boldsymbol{A}(\tau)]^2}{2} d\tau$, and the vector potential of the field is $\boldsymbol{A}(t) = -\int^t \boldsymbol{E}(t)dt$. The final expression of Green's function is

$$\tilde{G}_{v,h}(t,t') = -i\int d\boldsymbol{p}\Big|\phi_{\boldsymbol{p}}^{\rm V}(t)\Big\rangle\langle\boldsymbol{p}+\boldsymbol{A}(t')\Big|, \tag{9}$$

with three-dimensional integrations carried out over the canonical momentum in the calculation. In reality, there should be difference between Green's functions $\tilde{G}_v$ and $\tilde{G}_h$ because of the core-electron rearrangement. For example, the potential felt by the continuum electron varies when the core making transition from the valence shell to the inner shell. The difference is ignored in the present model.

The harmonic emission spectrum is obtained from the Fourier transformation of the induced dipole moment

along the laser polarization, which can be divided into three parts:

$$\boldsymbol{d}_v(t) = a_{\rm g}^*(t)e^{-iI_1\,t}(\langle\psi_1^{\rm D}|\boldsymbol{r}|\psi_v\rangle + \langle\varphi_1|\psi_v\rangle) + c.c, \quad (10)$$

$$\boldsymbol{d}_h(t) = a_{\rm g}^*(t)e^{-iI_2\,t}(\langle\psi_2^{\rm D}|\boldsymbol{r}|\psi_h\rangle + \langle\varphi_2|\psi_h\rangle) + c.c, \quad (11)$$

$$\boldsymbol{d}_x(t) = e^{-i\Delta I t}(\boldsymbol{d}_{12}\langle\psi_v|\psi_h\rangle + \boldsymbol{d}_{vh} + \boldsymbol{d}_{ex}) + c.c. \quad (12)$$

Here $\boldsymbol{d}_v(t)$ and $\boldsymbol{d}_h(t)$ are related to the paths v and h of HHG illustrated in Fig. 1, respectively. They both consist of an effective one-electron transition with the ionization channel-specific Dyson orbital $\psi_{1,2}^{\rm D} = \sqrt{n}\langle\Phi'_{1,2}|\Psi_{\rm g}\rangle'$, and an exchange correction term as introduced in Ref. [26] with $\varphi_{1,2} = \sqrt{n}\langle\Phi'_{1,2}|\sum_{i=1}^{n-1}\boldsymbol{r}_i|\Psi_{\rm g}\rangle'$. The path x of HHG is determined by the dipole moment $\boldsymbol{d}_x(t)$ from the transition between the two nonstationary states. The first term originates from the bound-bound transition among the two ionic states while the continuum makes jumping. The second term $\boldsymbol{d}_{vh} = \langle\Phi'_1\psi_v|\boldsymbol{r}|\Phi'_2\psi_h\rangle$ arises from the field-induced continuum-continuum transition between the two nostationary states. Because it usually gives rise to low frequency emission spectra, we neglect it here. The bound-continuum transition term $\boldsymbol{d}_{ex} = 2\sum_{i=1}^{n-1}\langle\hat{P}_{in}\Phi'_1\psi_v|\boldsymbol{r}|\Phi'_2\psi_h\rangle$ describes a two-step process as in Ref. [28], where the electron released from the valence orbital promotes the inner-shell electron to the vacancy it created upon recollision, and recombines into the newly formed hole to emit harmonics. This multi-electron collision plays a crucial role in strong-field ionization in the form of dynamical core polarization,[24,25,29,35] and manifest itself in high-harmonic generation.[26,28,29] However, compared to the XUV resonant excitation in this study, the probability of collision-induced rearrangement is small enough to be neglected.

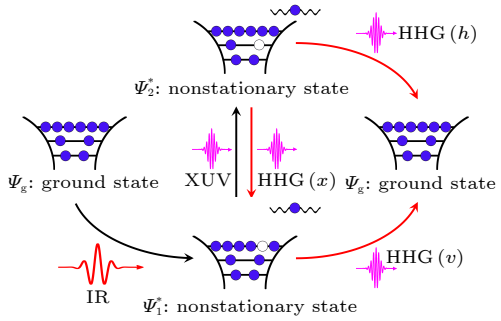

Fig. 1. Illustration of the interaction of the atom with the laser and XUV fields and the related high-harmonic generation processes: Ionization from the filled valence shell by the laser field creates the nonstationary state Ψ_1^* with its associated continuum ψ_v. Concurrently, it opens the subshell allowing the followed resonant transition pumped by the XUV pulse, which creates a hole in the core and transfers the continuum into ψ_h, i.e., to the nonstationary state Ψ_2^*. Recombination into the valence shell (path v) and the core hole (path h) could emit high-order harmonics. The resonant transition from the two nonstationary states (path x) also generates coherent harmonics.

To mimic the Ne atom, we choose the ionization potential of the valence shell as $I_1 = 21.56$ eV and the transition energy of $\Delta I = 26.89$ eV corresponding to $2s$ to $2p$ of the Ne atom. We use a laser pulse with one-cycle duration of 800 nm. In Fig. 2, the emission spectra calculated from the three individual processes are presented, as well as the total spectra, at the time delay of 0. The spectra directly calculated from $\boldsymbol{d}_v$ for the recombination into the valence shell are the same as those obtained without the XUV pulse which induces core-valence transition only.

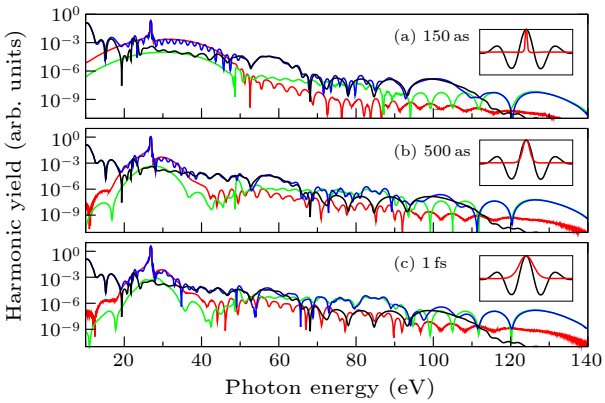

Fig. 2. Harmonic spectra calculated from $\boldsymbol{d}_v$ (black), $\boldsymbol{d}_x$ (red), $\boldsymbol{d}_h$ (green) and the total dipole moment $\boldsymbol{d}(t)$ (blue), at the time delay of 0 between the two pulses, at different XUV pulse durations of 150 as, 500 as, and 1 fs in (a)–(c). The electric field and the envelop of the APs are shown in the insets. The laser intensity is 4×10^{14} W/cm^2 and the XUV pulse intensity is 1×10^{13} W/cm^2 for all the cases.

In Fig. 2, it can be seen that the cutoff of the total spectra (blue lines) is extended compared to that emitted through path v (black lines). Once the hole in the inner shell is created, the electron can directly recombine into the hole through path h (green lines) and harmonics are emitted with the cut-off energy extended by ΔI, which has also been observed in HHG from multiple orbitals in molecules with ionization from one orbital and recombination to a lower-lying orbital, either coherent driven by strong IR field [36] or magnetic field.[37] For harmonics generated from path x (red lines), a pronounced peak appears at the core-valence transition energy. The total emission of harmonics (blue lines) around the resonance peak is enhanced by orders and therefore dominated by the path x. As the XUV pulse duration becomes shorter, the continuum background of the spectra becomes broader, however, the profile of the peak remains the same.

Note that the spectrum does not simply reflect the line shape of the core-valence transition, as seen by the higher energy photon of emission. The path x is in fact from the coherent transition between two nonstationary states Ψ_1^* and Ψ_2^*, similar to autoionization states with one electron embed in the continuum interacting loosely with the ionic core. Because of the driving of the external laser fields, the total energy of the nonstationary state is varying with time and spreading over a broad range due to the correlation between the continuum electron and the ion. Their energy difference gives rise to the emission of higher energy photon whose yields are determined by both the transition dipole of the ionic states and the temporal correlation between the two associated continua. When the contributions from all the three paths are comparable, their interference produces a generalized Fano profile (see the total emission around 70 eV), similarly to the

laser-assisted autoionization [38–40] where the autoionization profile evolves with the laser fields.

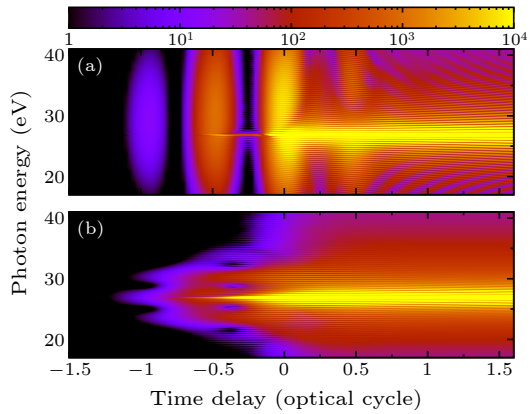

Fig. 3. Variation of the emission spectra induced by core-valence transition at different time delays between the IR pulse and APs with durations of (a) 150 as and (b) 1 fs.

By varying the time delay between the IR and the XUV pulses, the emission spectra from $\boldsymbol{d}_x$ changes as shown in Fig. 3 for the XUV pulse duration of 150 as and 1 fs. The spectra intensity is related to the vacancy in the valence shell induced by tunnelling ionization. The sensitivity of ionization to the instantaneous field leads to the strongly modulated delay-dependent emission spectra in Fig. 3. Especially, when the AP comes before the maximum of the IR field (negative delay), the ionization probability is small and the emission is very weak as the emission from core-valence transition is prohibited without ionization of the valence shell.

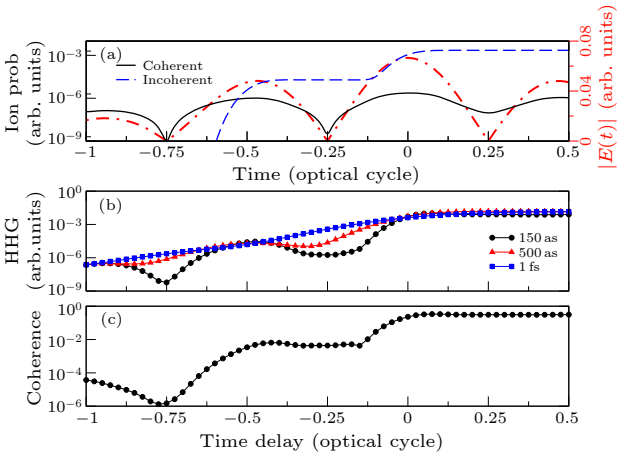

Fig. 4. (a) Dashed and solid lines represent the ionization probability obtained from incoherent integration of the ionization rate at each instantaneous field and from $||\psi_v||^2$, respectively. The dash-dotted line is the absolute value of the instantaneous electric field. (b) Harmonic emission yields integrated from 25.89 eV to 27.89 eV with AP durations of 150 as, 500 as, and 1 fs. (c) The coherence between the valence-hole and core-hole states.

In order to quantify the varying of emission with respect to the time delay, we integrate the total harmonic yields around the resonance peak over [25.89, 27.89] eV shown in Fig. 4(b) for different AP durations. The yields reach a local maximum whenever the laser field strength passes a local maximum. This is related to the fact that the ionization rate peaks at those instants and leaves more vacancy in the valence shell. Interestingly, the yields exhibit modulation with time delay, which is against the expectation that the ionization probability increases monochromatically when the incoherent ionization probability is calculated by integrating the ADK ionization rate over time [dashed lines in Fig. 4(a)]. In this case, the electron will never interact with its parent ion once excited to the continuum. On the other hand, the ionization probability obtained by the integral population of the continuum states $||\psi_v||^2$ at each instant exhibits modulation [solid lines in Fig. 4(a)], originating from the dynamical polarization of the laser-dressed nonstationary states, similar to the results in Ref. [10] that the modulation is observed in the attosecond transient absorption spectra and is attributed to the transient ground-state polarization.

To further understand the modulation of the harmonic yields, we calculate the coherence between the valence-hole and core-hole states. The coordinate representation of the density operator corresponds to these two nonstationary states is

$$\rho(\mu, \boldsymbol{r}', \nu, \boldsymbol{r}, t) = \langle \mu, \boldsymbol{r}'|\Psi(t)\rangle\langle\Psi(t)|\nu, \boldsymbol{r}\rangle, \tag{13}$$

with μ and ν representing the $(n-1)$-electron coordinates. We can define the reduced density matrix by integrating out the continuum electron coordinate, $\rho^{\rm c}_{\mu,\nu}(t) = \int d\boldsymbol{r}\rho(\mu, \boldsymbol{r}, \nu, \boldsymbol{r}, t)$. The coherence between the valence-hole and core-hole states is the nondiagonal term of the reduced density matrix on the basis of the cationic eigenstates:

$$\rho^{\rm c}_{12}(t) = \langle\Phi_1|\hat{\rho}^{\rm c}|\Phi_2\rangle, \tag{14}$$

which reflects the temporal correlation between the two continuum wave packets. The diagonal term of the reduced density matrix $\rho^{\rm c}_{11}$ ($\rho^{\rm c}_{22}$) represents the probability of the hole in the valence (inner) shell. The coherence between the valence-hole and core-hole states is shown in Fig. 4(c). Its behavior follows the harmonic yields with AP duration of 150 as. Because the longer the AP is, the more the time-averaged vacancy is probed, and the less the time-delayed sum yields are contrasted. As shown in Fig. 4(b), the emission yield turns into almost a smooth line for AP duration of 1 fs. More than probing the coherence of the valence-hole state, the AP probes the coherence transfer from the valence-hole to the core-hole state. During the propagation, the electron jumps between the two ionic state-associated continua because of the driving of the AP. Therefore, our two-color harmonic spectroscopy is capable of probing both the coherence of electron wavepacket induced by strong-field ionization and its transition between the valence-hole and core-hole states.

In conclusion, we have proposed an IR-pump-XUV-probe scheme to investigate the interplay of the valence-hole and core-hole states created from atoms with filled valence shells. Using the laser-induced ionization as a gate for XUV excitation of core electrons can provide us the opportunity to probe both the core and valence electron dynamics by manifesting themselves as a pronounced resonant peak in harmonic spectra and an extended cut-off harmonic emission. The coherent interplay of multiple

paths of HHG is found to be evident in the harmonic spectra. By analyzing the modulation of the spectra with the time delay between the IR field and the AP, we show that the coherence of the ionization process and the driven core-hole and valence-hole coherence contribute to HHG which can be utilized to obtain the multi-electron-hole or multichannel coherent information. Our work is also applicable to further investigation on ionization-coupled multi-electron dynamics, such as the exchange correlation effects or core-excitation dynamics.

Acknowledgments. This work was supported by the Major Research Plan of the National Natural Science Foundation of China (Grant No. 91850201), the National Key Research and Development Program of China (Grant No. 2019YFA0307703), and the National Natural Science Foundation of China (Grant Nos. 11874066 and 11804388).

References

[1] Goulielmakis E, Loh Z H, Wirth A, Santra R, Rohringer N, Yakovlev V S, Zherebtsov S, Pfeifer T, Azzeer A M, Kling M F, Leone S R, and Krausz F 2010 *Nature* **466** 739
[2] Ott C, Kaldun A, Argenti L, Raith P, Meyer K, Laux M, Zhang Y, Blattermann A, Hagstotz S, Ding T, Heck R, Madronero J, Martin F, and Pfeifer T 2014 *Nature* **516** 374
[3] McFarland B K, Farrell J P, Miyabe S *et al.* 2014 *Nat. Commun.* **5** 4235
[4] Young L, Kanter E P, Krässig B *et al.* 2010 *Nature* **466** 56
[5] Erk B, Boll R, Trippel S *et al.* 2014 *Science* **345** 288
[6] Schultze M, Fieß M, Karpowicz N *et al.* 2010 *Science* **328** 1658
[7] Huang Y, Zhao J, Shu Z, Zhu Y, Liu J, Dong W, Wang X, Lü Z, Zhang D, Yuan J, Chen J, and Zhao Z 2021 *Ultrafast Sci.* **2021** 9837107
[8] Lépine F, Ivanov M Y, and Vrakking M J 2014 *Nat. Photon.* **8** 195
[9] Sabbar M, Heuser S, Boge R, Lucchini M, Carette T, Lindroth E, Gallmann L, Cirelli C, and Keller U 2015 *Phys. Rev. Lett.* **115** 133001
[10] Sabbar M, Timmers H, Chen Y J, Pymer A K, Loh Z H, Sayres S, Pabst S, Santra R, and Leone S R 2017 *Nat. Phys.* **13** 472
[11] Leone S R, McCurdy C W, Burgdörfer J *et al.* 2014 *Nat. Photon.* **8** 162
[12] Golubev N V and Kuleff A I 2015 *Phys. Rev. A* **91** 051401
[13] Obara Y, Ito H, Ito T, Kurahashi N, Thürmer S, Tanaka H, Katayama T, Togashi T, Owada S, Yamamoto Y I, Karashima S, Nishitani J, Yabashi M, Suzuki T, and Misawa K 2017 *Struct. Dyn.* **4** 044033
[14] Wörner H J, Arrell C A, Banerji N, Cannizzo A, Chergui M, Das A K, Hamm P, Keller U, Kraus P M, Liberatore E, Lopez-Tarifa P, Lucchini M, Meuwly M, Milne C, Moser J E, Rothlisberger U, Smolentsev G, Teuscher J, van Bokhoven J A, and Wenger O 2017 *Struct. Dyn.* **4** 061508
[15] Rohringer N and Santra R 2009 *Phys. Rev. A* **79** 053402
[16] Emma P, Akre R, Arthur J *et al.* 2010 *Nat. Photon.* **4** 641
[17] Rohringer N, Ryan D, London R A, Purvis M, Albert F, Dunn J, Bozek J D, Bostedt C, Graf A, Hill R, Hau-Riege S P, and Rocca J J 2012 *Nature* **481** 488
[18] Paul P M, Toma E S, Breger P, Mullot G, Augé F, Balcou P, Muller H G, and Agostini P 2001 *Science* **292** 1689
[19] Hentschel M, Kienberger R, Spielmann C, Reider G A, Milosevic N, Brabec T, Corkum P, Heinzmann U, Drescher M, and Krausz F 2001 *Nature* **414** 509
[20] Zhao K, Zhang Q, Chini M, Wu Y, Wang X, and Chang Z 2012 *Opt. Lett.* **37** 3891
[21] Li Y, Gao C, Dong W, Zeng J, and Yuan J 2015 arXiv:1501.02660 [physics.atom-ph]
[22] Rackstraw D S, Ciricosta O, Vinko S M *et al.* 2015 *Phys. Rev. Lett.* **114** 015003
[23] Fukuzawa H, Son S K, Motomura K *et al.* 2013 *Phys. Rev. Lett.* **110** 173005
[24] Zhang B, Yuan J, and Zhao Z 2013 *Phys. Rev. Lett.* **111** 163001
[25] Zhao Z X and Yuan J M 2014 *Phys. Rev. A* **89** 023404
[26] Patchkovskii S, Zhao Z, Brabec T, and Villeneuve D M 2006 *Phys. Rev. Lett.* **97** 123003
[27] Santra R and Gordon A 2006 *Phys. Rev. Lett.* **96** 073906
[28] Pabst S and Santra R 2013 *Phys. Rev. Lett.* **111** 233005
[29] Zhang B, Yuan J, and Zhao Z 2014 *Phys. Rev. A* **90** 035402
[30] Leeuwenburgh J, Cooper B, Averbukh V, Marangos J P, and Ivanov M 2013 *Phys. Rev. Lett.* **111** 123002
[31] Leeuwenburgh J, Cooper B, Averbukh V, Marangos J P, and Ivanov M 2014 *Phys. Rev. A* **90** 033426
[32] Uzan A J, Soifer H, Pedatzur O, Clergerie A, Larroque S, Bruner B D, Pons B, Ivanov M, Smirnova O, and Dudovich N 2020 *Nat. Photon.* **14** 188
[33] Shu Z, Liang H, Wang Y, Hu S, Chen S, Xu H, Ma R, Ding D, and Chen J 2022 *Phys. Rev. Lett.* **128** 183202
[34] Lewenstein M, Balcou P, Ivanov M Y, L'Huillier A, and Corkum P B 1994 *Phys. Rev. A* **49** 2117
[35] Rapp J and Bauer D 2014 *Phys. Rev. A* **89** 033401
[36] Mairesse Y, Higuet J, Dudovich N, Shafir D, Fabre B, Mevel E, Constant E, Patchkovskii S, Walters Z, Ivanov M Y, and Smirnova O 2010 *Phys. Rev. Lett.* **104** 213601
[37] Cireasa R, Boguslavskiy A, Pons B *et al.* 2015 *Nat. Phys.* **11** 654
[38] Zhao Z X and Lin C D 2005 *Phys. Rev. A* **71** 060702
[39] Wickenhauser M, Burgdörfer J, Krausz F, and Drescher M 2005 *Phys. Rev. Lett.* **94** 023002
[40] Zielinski A, Majety V P, Nagele S, Pazourek R, Burgdörfer J, and Scrinzi A 2015 *Phys. Rev. Lett.* **115** 243001